JOURNAL OF MATERIALS SCIENCE 32 (1997) 997–1004

# The relationship between microstructure and Young's modulus of thermally sprayed ceramic coatings

CHANGJIU LI
*Welding Research Institute, School of Mechanical Engineering, Xi' an Jiaotong University, Xi' an, Shaanxi, 710049, People's Republic of China*

AKIRA OHMORI
*Welding Research Institute, Osaka University, 11-1 Mihogaoka, Ibaraki, Osaka, 567 Japan*

R. MCPHERSON
*CSIRO Division of Manufacturing Technology, Preston, 3072, Victoria, Australia*

An idealized model for the microstructure of thermally sprayed ceramic coatings, consisting of the stacking of lamellae a few micrometres thick, has been used to estimate Young's modulus of the coating perpendicular to the coating plane. A theoretical relationship between Young's modulus and the microstructural parameters has been established. There are two components of elastic strain of the coating under tensile stress, one arising from localized elastic strain at the regions of real-bonded area between lamellae, and the other arising from elastic bending of the lamellae between bonded regions. The bending component only becomes significant for a percentage bonding ratio between lamellae of less than 40%. The bending strain contribution depends strongly upon geometrical parameters of the coating microstructure. The estimated Young's modulus for a typical alumina coating, based on quantitative microstructural data, was about 24% of that for the fully dense material. Taking into account the variable proportion of $\alpha$-$Al_2O_3$ and $\gamma$-$Al_2O_3$ forms in an alumina coating, the comparison of the estimated Young's modulus with published data gives reasonable agreement for the coating prepared over a wide range of processes and experimental conditions.

## 1. Introduction

The mechanical properties of materials are generally a sensitive function of their microstructure and the relationship between microstructure and properties therefore forms a central theme of materials science. Although similar considerations can undoubtedly be applied to thermally sprayed coatings, there has been relatively little study of this technologically-significant topic. The microstructure of thermally sprayed coatings is markedly different to conventionally processed materials since they consist of rapidly solidified lamellae formed by the impact of a succession of molten droplets. An important feature of ceramic coating microstructure is the presence of a complex network of pores associated with imperfect contact between lamellae, microcracks within lamellae and the incorporation of partly melted particles. The microstructure is therefore strongly related to the mechanics of coating formation and may be regarded as the major link between processing parameters and coating properties [1].

The elastic moduli, which relate the reversible deformation of materials to applied stress, are basic parameters associated with mechanical behaviour. Two moduli are required to describe the stress–strain behaviour of an isotropic material and Young's modulus ($E$) and Poisson's ratio ($v$) are normally used in an engineering context. The Young's modulus of a dense, isotropic, single phase solid is generally regarded as largely microstructure independent and related to the forces between the constituent atoms or ions. For dense, multi-phase solids with an isotropic microstructure, $E$ may be simply related to the volume fraction of the phases and their respective moduli. The Young's modulus of many porous materials, that is, two phase structures in which the second phase has $E = 0$, is found to conform to empirical relationships such as $E = E_0 \exp(-bp)$, where $E_0$ is the modulus of the dense material, $p$ the volume fraction porosity and $b$ a constant [2]. The pore morphology and distribution may, however, have an additional influence on Young's modulus. An analysis for a solid containing pores in the form of oriented spheroids indicates a large reduction in Young's modulus at small porosity for disc-shaped pores, oriented with their diameter perpendicular to the stress axis, compared with a distribution of spherical pores at the same total porosity. For example, at 5% porosity $E$ is reduced to $0.34E_0$

0022–2461  

for a pore diameter-to-thickness ratio of 10, compared to $0.90E_0$ for spherical pores [3].

A number of experimental studies have shown that the Young's modulus of a thermally sprayed coating is very much lower than that observed for the same material, at similar porosity, prepared by conventional processes [4–9]. This large reduction in modulus has been ascribed to a microstructural effect associated with limited "true" contact between the lamellae of which the coating is constituted [10]. At an estimated true contact of $\sim$25% the apparent interlamellar contact was found to be consistent with published elastic modulus and thermal conductivity data [11]. The imperfect interlamellar contact hypothesis has recently been confirmed experimentally by an electroplating technique which reveals the porosity substructure in plasma sprayed ceramic coatings [12, 13]. Quantitative analysis of this substructure for plasma sprayed alumina coatings revealed the following relationships between the spraying conditions and features of the microstructure [14].

(a) The mean lamellar thickness remained approximately constant (1.5 to 2 μm), at a constant torch power of 28 kW as a function of spray distance up to 150 mm, but increased beyond this to $\sim$3 μm at 200 mm.

(b) The mean lamellar thickness remained approximately constant (1.5 to 2 μm), for a spray distance of 100 mm, over the power range 21 to 32 kW.

(c) The mean bonding ratio (fraction real contact area between lamellae) increased from $\sim$24% at a torch power of 21 kW to a saturation level of 32% at powers greater than 25 kW (spraying distance 100 mm).

(d) The mean bonding ratio decreased to less than 20% at spray distances greater than 100 mm (torch power 28 kW).

(e) The vertical crack density within lamellae decreased from $\sim$1.5 per 10 μm at a spraying distance of 100 mm to $\sim$1 per 10 μm at spraying distances 150 $\sim$ 200 mm (torch power 28 kW).

(f) The vertical crack density increased with torch power from $\sim$1 per 10 μm at 21 kW to $\sim$1.75 per 10 μm at 32 kW at a spray distance of 100 mm.

A study of the stress–strain behaviour of plasma sprayed alumina coatings (open porosity $\sim$4%, $\alpha$-$Al_2O_3$ content $\sim$10%) perpendicular and parallel to the coating plane indicated that they exhibited planar elastic anisotropy, a result not unexpected considering the lamellar microstructure of thermally sprayed coatings [15]. It should be noted that five independent moduli are required to describe planar elastic anisotropy. Although the stress–strain curves were linear elastic in the coating plane, non-linear elastic behaviour was observed in tension perpendicular to the coating plane. Similar non-linear elastic behaviour has also been observed in plasma sprayed Ni–Al coatings in which the Young's modulus perpendicular to the coating plane was $\sim$40% of that observed for an electroplated Ni coating, in good agreement with the fraction interlamellar contact estimated from porosity measurements [16]. The non-linear elastic behaviour observed in these coatings was ascribed to the opening of interlamellar pores initially clamped together by residual stresses.

The present paper examines the elastic response of the idealized lamellar structure of a thermally sprayed coating in more detail using circular plate bending theory.

## 2. The coating microstructural model

The structure of a flattened particle in a typical plasma sprayed alumina coating, derived from studies using the copper plating technique is illustrated in Fig. 1 [12–14]. An idealized coating structure based on this, for the purpose of analysis of elastic behaviour is shown in Fig. 2. It is assumed to consist of a random stacking of circular lamellae of mean thickness $\delta$, each of which contains a network of orthogonal microcracks perpendicular to the lamellar plane with mean crack width $x$ and spacing $y$. True contact between lamellae occurs at circular regions, radius $a$, with mean fraction true contact (bonding ratio) between lamellae $\alpha$.

It is also assumed that the structure consists of parallel lamellar layers with identical thickness and that the individual bonded areas, radius $a$, between adjacent lamellae are uniformly distributed along the interface; the tortuosity of the lamellae is neglected.

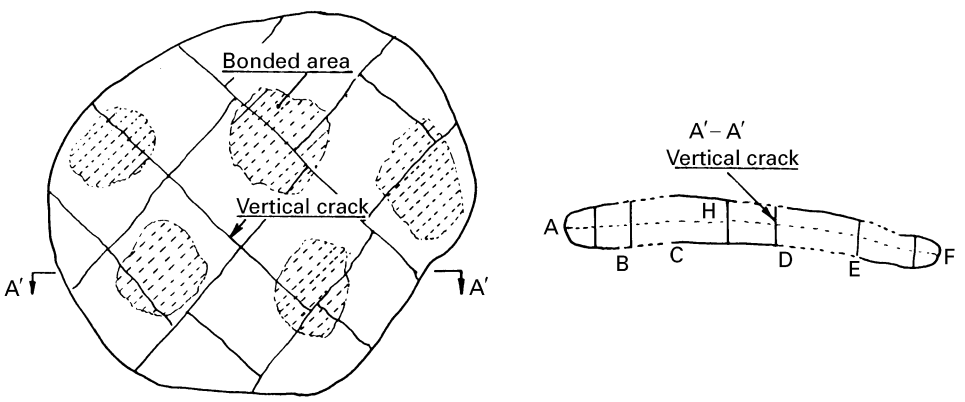


*Figure 1* Schematic diagrams of the structure of a flattened ceramic particle in a coating and bonding to the coating: (a) top view and (b) a cross-section (– – – – bonded interface, —— non-bonded interface) [12, 13].

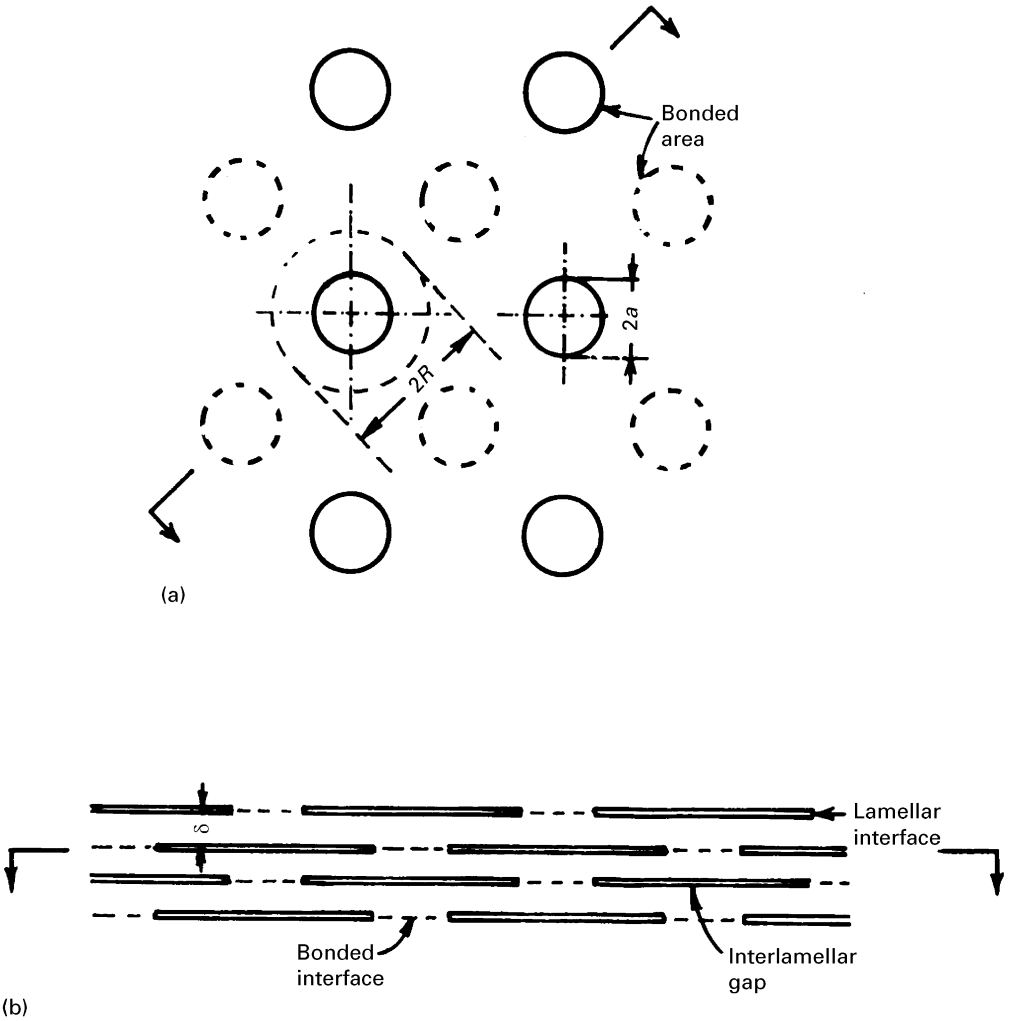


*Figure 2* Idealized model of coating structure: (a) plan view of lamellar interface and (b) cross-section of coating.

## 3. Mechanical behaviour of the model structure under load

When a load is applied to the coating in the direction perpendicular to the coating plane, the force must be transferred from one surface of the coating to the other through the bonded regions between lamellae. Thus there is localized elastic strain at the bonded regions and elastic deflection of the lamellae in the non-bonded regions between them. The following assumptions are made.

1. The bonded area is rigid and does not deflect under stress.
2. The lamellae deflect elastically in the unbonded regions.
3. The effects of stress concentration at the periphery of the bonded regions are neglected.
4. The effects of vertical microcracks in the lamellae and the periphery of the lamellae are neglected.

The total displacement under stress for a single layer in the coating is then the result of bending of the unbonded area plus displacement at the bonded area. The displacement for a single layer will be that between points A and B as shown in Fig. 3.

If the stress applied to the coating perpendicular to the coating plane is $\sigma$, the real stress applied to the contact regions will be:

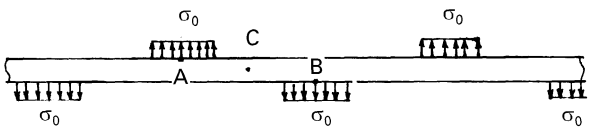


*Figure 3* Loading between lamellae by stress $\sigma_0$ at bonded regions.

$$\sigma_0 = \sigma/\alpha \quad (1)$$

Supposing $\Delta l$ is the total displacement of a single lamella then

$$\Delta l = 2(\Delta l' + f) \quad (2)$$

where $\Delta l'$ is the displacement of point A with respect to central plane of the lamellae, and $f$ is the deflection at point C with respect to A. Therefore, the apparent strain ($\varepsilon$) in the coating becomes:

$$\varepsilon = \Delta l/\delta \quad (3)$$

and the apparent Young's modulus ($E_c$) of the coating:

$$E_c = \sigma/\varepsilon \quad (4)$$

The loading on a single bonded region can be simplified as a circular plate bending as shown in Fig. 4

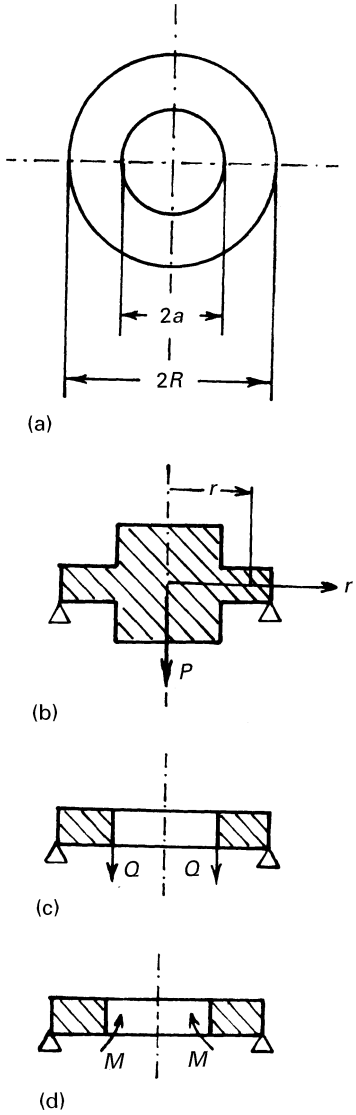


*Figure 4* Mechanical model for deflection of lamellae between bonded regions.

and the displacement and deflection may be calculated as follows [17].

## 3.1. Displacement ($\Delta l'$)

The loading for the bonded region may be considered as shown in Fig. 5. The stress $\sigma_0$ is uniformly distributed along the bonded interface. The shear stress ($\tau$) is assumed to be uniformly distributed along the outer circular cross-section of the bonded region. The stress $\sigma'_x$ exerted along the cross-section parallel to the bonded interface is a function of the position on the cross-section ($x$). From the following relationship:

$$\pi a^2 \sigma'_z = \pi a^2 \sigma_0 - 2\pi a \tau x$$

and using condition $x = \delta$, $\sigma'_x = 0$, we obtain:

$$\sigma'_x = \sigma_0(1 - x/\delta)$$

$$\varepsilon'_x = \sigma'_x / E$$

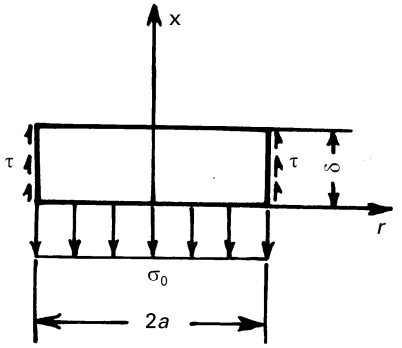


*Figure 5* Stress distribution in bonded region.

where $E$ is Young's modulus of the lamellar material. The total displacement $\Delta l'$ becomes:

$$\Delta l' = \int_0^\delta \varepsilon'_x \, dx = \int_0^\delta \frac{\sigma_0}{E}(1 - x/\delta)\, dx = \frac{\sigma_0 \delta}{2E} \quad (5)$$

## 3.2. Calculation of deflection ($f$)

The deflection for a single bonded region on loading can be calculated from the case of bending of a circular plate in which the load is applied through the central, rigid, bonded area and the outer edge is simply supported because the differential of the slope of deflection at point c is zero. This may be considered as the combination of the loading shown in Fig. 4c, in which the load is built in along the inner edge, uniformly loaded along the outer edge, and the case shown in Fig. 4d, in which only the bending moment is uniformly applied along the inner edge under the condition that the slope at the built-in edge is zero because of the rigidity of the bonded area.

For the case shown in Fig. 4c, the maximum deflection produced by load $P$ can be obtained as follows (see Appendix I):

$$f_p = \frac{PR^2}{8\pi D}\left[\left(1 + \frac{1}{2}\frac{1-v}{1+v}\right)\left(\frac{\beta^2 - 1}{\beta^2}\right) + \frac{1+v}{1-v}\frac{2}{\beta^2 - 1}\ln^2 \beta\right] \quad (6)$$

where

$$D = \frac{E\delta^3}{12(1 - v^2)}, \quad \beta = \frac{R}{a}$$

$E$ and $v$ are Young's modulus and Poisson's ratio of lamellae plate, respectively.

Therefore, we obtain:

$$f_p = \frac{PR^2}{E\delta^3}\frac{3(1-v^2)}{2\pi}\left[\left(1 + \frac{1}{2}\frac{1-v}{1+v}\right)\left(\frac{\beta^2 - 1}{\beta^2}\right) + \frac{1+v}{1-v}\frac{2}{\beta^2 - 1}\ln^2 \beta\right] = \frac{PR^2}{E\delta^3} f_1(\beta) \quad (7)$$

$$f_1(\beta) = \frac{3(1-v^2)}{2\pi}\left[\left(1+\frac{1}{2}\frac{1-v}{1+v}\right)\left(\frac{\beta^2-1}{\beta^2}\right) + \frac{1+v}{1-v}\frac{2}{\beta^2-1}\ln^2\beta\right] \quad (8)$$

For the case shown in Fig. 4d, the maximum deflection becomes:

$$f_m = -\left[\frac{1}{2(1+v)\beta^2} + \frac{\ln\beta}{(1-v)(\beta^2-1)}\frac{MR^2}{D}\right] \quad (9)$$

From the condition that the slope at the built in edge is zero:

$$M = \frac{P}{4\pi}\frac{(1-v)(\beta^2-1)+2(1+v)\beta^2\ln\beta}{(1+v)\beta^2+(1-v)} \quad (10)$$

Substituting this in Equation 9 we obtain:

$$f_m = -\frac{PR^2}{4\pi D}\frac{[(1-v)(\beta^2-1)+2(1+v)\beta^2\ln\beta]^2}{[(1+v)\beta^2+(1-v)]} \times\frac{1}{2(1-v^2)\beta^2(\beta^2-1)} \quad (11)$$

From

$$D = \frac{E\delta^3}{12(1-v^2)}$$

$$f_m = -\frac{3PR^2}{2\pi E\delta^3}\frac{[(1-v)(\beta^2-1)+2(1+v)\beta^2\ln\beta]^2}{\beta^2(\beta^2-1)[(1+v)\beta^2+(1-v)]} = -\frac{PR^2}{E\delta^3}f_2(\beta) \quad (12)$$

where

$$f_2(\beta) = \frac{3}{2\pi}\frac{[(1-v)(\beta^2-1)+2(1+v)\beta^2\ln\beta]^2}{\beta^2(\beta^2-1)[(1+v)\beta^2+(1-v)]} \quad (13)$$

The total deflection becomes:

$$f = f_p + f_m = \frac{PR^2}{E\delta^3}[f_1(\beta)-f_2(\beta)] \quad (14)$$

### 3.3. Apparent Young's modulus of coating

The total displacement $\Delta l$ becomes:

$$\Delta l = 2(f+\Delta l') = 2\left\{\frac{PR^2}{E\delta^3}[f_1(\beta)-f_2(\beta)] + \frac{\sigma_0\delta}{2E}\right\} \quad (15)$$

Substituting this in Equation 3 we obtain the apparent coating strain:

$$\varepsilon = \frac{\Delta l}{\delta} = \frac{\sigma_0}{E} + \frac{2PR^2}{E\delta^4}[f_1(\beta)-f_2(\beta)] \quad (16)$$

Noting that $P = \pi a^2\sigma_0$

$$\varepsilon = \frac{\sigma_0}{E}\left\{1+\frac{2\pi a^2R^2}{\delta^4}[f_1(\beta)-f_2(\beta)]\right\} = \frac{\sigma_0}{E}\left\{1+2\pi\left(\frac{a}{\delta}\right)^4\beta^2[f_1(\beta)-f_2(\beta)]\right\} \quad (17)$$

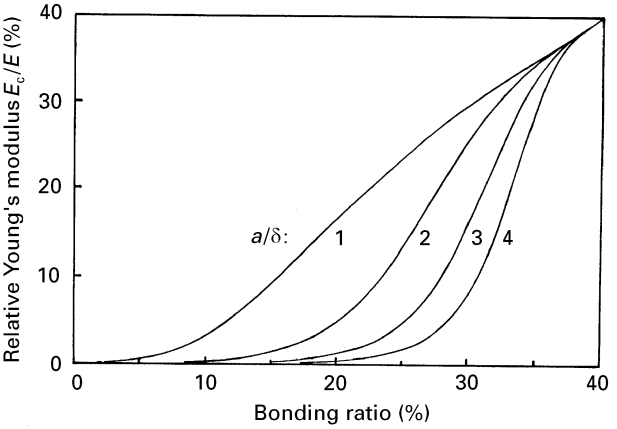


*Figure 6* Relation between relative Young's modulus ($E_c/E_0$) and lamellar bonding ratio as a function of $a/\delta$. Poisson's ratio is 0.25.

Substituting Equation 1 and Equation 17 into Equation 4, we obtain:

$$E_c = \frac{\sigma}{\varepsilon} = \alpha E\left\{1+2\pi\left(\frac{a}{\delta}\right)^4\beta^2[f_1(\beta)-f_2(\beta)]\right\}^{-1} \quad (18)$$

Therefore, the relative Young's modulus perpendicular to the coating plane with respect to the modulus of the dense material is:

$$\frac{E_c}{E} = \alpha\left\{1+2\pi\left(\frac{a}{\delta}\right)^4\beta^2[f_1(\beta)-f_2(\beta)]\right\}^{-1} \quad (19)$$

Note that deflection owing to bending only takes place under the following condition:

$$R > a \quad (20)$$

From the relation:

$$R = a/2(\pi/2\alpha)^{1/2} \quad (21)$$

we obtain that Equation 18 is valid when the mean bonding ratio between lamellae is less than 40%, by letting $R = a$. When $\alpha$ is larger than 40%, the deflection by bending can be neglected. Therefore we obtain:

$$E_c/E = \alpha \qquad (\alpha \geqslant 40\%) \quad (22)$$

The relationship between $E_c/E$ and the interlamellar bonding ratio as a function of $a/\delta$ is illustrated in Fig. 6.

## 4. Discussion

The analysis shows that the Young's modulus of the idealized model of a thermally sprayed coating perpendicular to the coating plane has two components: one related to the localized elastic deformation at bonded regions between lamellae, which is directly proportional to the bonding ratio or fraction real contact area between lamellae, and another related to bending of lamellae between bonded regions. The latter effect only becomes significant for a bonding ratio of less than $\sim$40% and depends strongly on the ratio of the mean dimension of the individual contact regions ($a$) to the mean lamellar thickness ($\delta$).

Measurements of the microstructural parameters of plasma sprayed alumina coatings, using the copper plating technique, have shown that a maximum mean bonding ratio is achieved as the spraying power is increased beyond 25 kW for torch–substrate distances of 80–120 mm; at larger distances the deposition efficiency and bonding ratio both decrease. The mean lamellar thickness remains constant at 1.5–2 μm for spray distances of 80–150 mm and is largely independent of torch power. The mean radius of the real contact region is approximately 5 μm [14].

Using these values we obtain from Fig. 6 ($a/\delta = 3$, $\alpha = 32\%$) the result $E_c/E = 24\%$. Without the contribution from lamellar bending $E_c/E$ would be 32%, that is, equal to the mean bonding ratio.

Although several studies of the elastic moduli of thermally sprayed alumina coatings have been reported, their interpretation is complicated because the materials have not always been well characterized and a variety of measurement techniques have been employed (Table I).

Unfortunately, interpretation of the data is also more difficult because coatings consist of a mixture of the stable $\alpha$-$Al_2O_3$ and metastable $\gamma$-$Al_2O_3$ forms, the proportions of which depend upon the spraying conditions since $\gamma$-$Al_2O_3$ is formed by the rapid solidification of completely molten droplets and $\alpha$-$Al_2O_3$ arises from the incorporation of incompletely melted particles [18]. The Young's modulus of completely dense $\alpha$-$Al_2O_3$ is $\sim$400 GPa [19] but that of $\gamma$-$Al_2O_3$ cannot be measured directly because of the unavailability of dense bulk specimens. The Young's modulus of $\gamma$-$Al_2O_3$ would be expected to be comparable with that of spinel ($MgO \cdot Al_2O_3$), 241 GPa [19], which has the same crystal structure but with 2/3rds of the $Mg^{2+}$ sites occupied by $Al^{3+}$. It is possible to estimate the compressibility ($\beta$) of solid solutions formed from pure compounds from the relationship [20]:

$$V_j\beta_j = \sum_{i=1}^{n} X_i V_i \beta_i \qquad (23)$$

where, $V_j$ = molar volume of solution of composition $j$, $V_i$ = molar volume and $X_i$ = mole fraction of the $i$th component of the solution. This relationship may be used to estimate $V_j\beta_j$ for $\gamma$-$Al_2O_3$ by extrapolation of experimental data for spinel-alumina solid solutions to pure alumina. This gives a value of 1.42 for the ratio of $(V\beta)_{spinel}$:$(V\beta)_\gamma$ and, taking into account the molar volumes, $\beta_\gamma/\beta_{spinel} = 0.98$. Since the bulk modulus, $B = 1/\beta$ and $E = 3B(1 - 2v)$, an estimated $E_\gamma/E_{spinel} = 1.02$ is arrived at assuming $v$ is the same for both phases, that is, an estimated Young's modulus for $\gamma$-$Al_2O_3$ of 246 GPa.

Another factor to consider is the apparent elastic anisotropy of thermally sprayed coatings as observed by McPherson and Cheang [15]. Their measurements of the Young's modulus of plasma sprayed coatings perpendicular and parallel to the coating plane, gave values of 29 and 88 GPa, respectively, with non-linear elastic behaviour in tension perpendicular to the coating plane. If these results are correct it means that the values reported in the literature are averages which depend upon the measurement technique employed.

TABLE I Reported values of Young's modulus of thermally sprayed alumina coatings

| Young's modulus (GPa) | % $\alpha$-$Al_2O_3$ | Porosity (%) | Spraying process | Reference |
|---|---|---|---|---|
| 34–40 | 0 | 8–10 | Flame | 4 |
| 15–28 | $\sim$33 | – | Plasma | 5 |
| 39 | – | 3 | Plasma | 6 |
| 31 | – | 23 | Plasma | 7 |
| 54 | 5–20 | – | Plasma | 8 |
| 20–50 | 0 | 7.5–11 | Flame | 9 |
| 60–90 | 25–34 | 14–16 | Plasma | 9 |

Fig. 6 shows that, for the idealized lamellar microstructure, the lamellar bending contribution becomes much more important and $E_c$ rapidly decreases as the bonding ratio falls below $\sim$40%. An important feature of these results is the large effect on modulus of microstructural factors such as mean lamellar thickness, mean contact region diameter and spacing over the range of bonding areas observed in practical coatings.

Applying the results to alumina coatings entirely of $\gamma$-$Al_2O_3$, with estimated Young's modulus of 250 GPa, and using previously measured microstructural data, gives the result shown in Fig. 7 (0% $\alpha$-$Al_2O_3$). The presence of $\alpha$-$Al_2O_3$ (Young's modulus 400 GPa) in alumina coatings would be expected to increase their modulus. One approach to estimating this effect is to substitute a weighted mean modulus of the two phases for $E_0$ in the calculation but this assumes that both phases are distributed as similar lamellae in the microstructure whereas the $\alpha$-$Al_2O_3$ is present in plasma sprayed coatings as spherical particles, arising from the incorporation of partly melted material, in a matrix of lamellar $\gamma$-$Al_2O_3$ [10]. Another approach is to estimate a modulus for the coating based on a weighted mean of the moduli of lamellar $\gamma$-$Al_2O_3$ (from Fig. 6) and dense $\alpha$-$Al_2O_3$, but this assumes perfect bonding between the $\alpha$-$Al_2O_3$ inclusions and the matrix which is unlikely. A more reasonable approach is to estimate the modulus for a mixture of lamellar $\gamma$-$Al_2O_3$, taking into account their elastic deflection from Fig. 6, and $\alpha$-$Al_2O_3$ using the same mean bonding ratio, that is, with no lamellar deflection component. The results for this case are shown in Fig. 7 for coatings containing 0, 10, 20 and 30 volume per cent $\alpha$-$Al_2O_3$. As shown, the latter approach gives values of Young's modulus for coatings with bonding ratios from 26 to 34% and $\alpha$-$Al_2O_3$ contents from 0 to 30 vol % which covers the rather wide range of values reported in the literature.

Although the proposed model is in qualitative agreement with published data, no account has been taken of the microcrack network present in ceramic lamellae, the planar anisotropy of properties to be expected from the lamellar microstructure, or the convoluted structure of lamellae. A more complete experimental study would require a quantitative

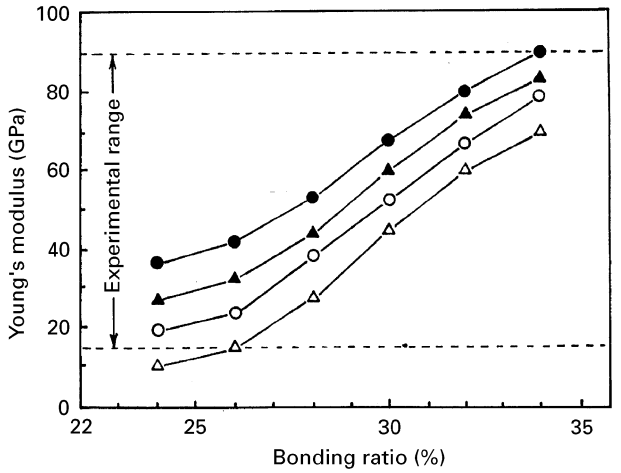


*Figure 7* Estimated Young's modulus of alumina coating as a function of bonded ratio and percentage $\alpha$-$Al_2O_3$ as unmelted particles. Range of experimental values from the literature are shown by dahsed lines. Key: $\alpha$-$Al_2O_3$ content; △ 0%; ○ 10%; ▲ 20% and ● 30%.

microstructural analysis of coatings prepared from a material which does not undergo a phase change during spraying, combined with determination of their elastic constants in the coating plane and perpendicular to it.

## 5. Conclusions

The relationship between the Young's modulus perpendicular to the coating plane and the microstructure of thermally sprayed ceramic coating has been theoretically established using an idealized microstructural model consisting of the stacking of lamellae a few micrometres thick and flat circular plate theory. There are two components of the elastic strain of the coating under tensile stress, one arising from localized elastic strain at regions of "true" contact between lamellae and the other arising from elastic bending of the lamellae between the contact regions. The bending component only becomes significant for percentage true contact between lamellae (bonding ratio) of less than 40%. The bending strain contribution depends strongly upon geometrical parameters of the coating microstructure. The estimated Young's modulus for a "typical" alumina coating, based on quantitative metallographic data, was $\sim$24% that of the fully dense material. Comparison with published data for alumina is complicated by the fact that practical coatings consist of a variable proportion of the $\alpha$- and $\gamma$-forms of $Al_2O_3$, and taking this into account, using an estimated value for the Young's modulus of $\gamma$-$Al_2O_3$, gives reasonable agreement with published values for thermally-sprayed coatings prepared using a range of processes and experimental conditions.

## Appendix A

The differential equation for the deflection of a circular plate symmetrically loaded as shown in Fig. 4 is:

$$\frac{\mathrm{d}}{\mathrm{d}r}\left[\frac{1}{r}\frac{\mathrm{d}}{\mathrm{d}r}\left(r\frac{\mathrm{d}w}{\mathrm{d}r}\right)\right] = \frac{Q}{D} \tag{A1}$$

where $w$ is the deflection at radius $r$ from axis of plate in the downward direction, $r$ is the radius at which deflection is considered. $Q$ is the shearing force per unit circumferential length at radius $r$ and $D$ is the flexural rigidity of the plate $= E\delta^3/12(1-v^2)$. For the case illustrated in Fig. 4c, where a load $P$ is uniformly distributed along the edges, $Q = P/2\pi r$. Substituting $Q$ in Equation A1 and integrating, we obtain:

$$w = \frac{Pr^2}{8\pi D}\left(\ln\frac{r}{R} - 1\right) + \frac{r^2}{4}C_1 + C_2\ln\frac{r}{R} + C_3 \tag{A2}$$

From the following boundary conditions for Fig. 4c, we can determine the integration constants $C_1, C_2$ and $C_3$. When

$$\begin{aligned} r &= R,\ w = 0 \\ r &= R,\ (M_1)_{r=R} = 0 \\ r &= a,\ (M_1)_{r=a} = 0 \end{aligned} \tag{A3}$$

where $M_1$ is the radial bending moment per unit length. From plate theory:

$$M_1 = -D\left(\frac{\mathrm{d}^2w}{\mathrm{d}r^2} + \frac{v}{r}\frac{\mathrm{d}w}{\mathrm{d}r}\right) \tag{A4}$$

From Equation A2 we obtain:

$$\frac{\mathrm{d}w}{\mathrm{d}r} = \frac{Pr}{4\pi D}\ln\frac{r}{R} - \frac{Pr}{8\pi D} + \frac{rC_1}{2} + \frac{C_2}{r} \tag{A5}$$

$$\frac{\mathrm{d}^2w}{\mathrm{d}r^2} = \frac{P}{4\pi D}\ln\frac{r}{R} + \frac{P}{8\pi D} + \frac{C_1}{2} - \frac{C_2}{r^2} \tag{A6}$$

Using these conditions we obtain:

$$\begin{aligned} C_1 &= \frac{P}{4\pi D}\left(\frac{2a^2}{R^2-a^2}\ln\frac{a}{R^2} - \frac{1-v}{1+v}\right) \\ C_2 &= \frac{P}{4\pi D}\frac{1+v}{1-v}\frac{R^2a^2}{R^2-a^2}\ln\frac{a}{R} \\ C_3 &= \frac{PR^2}{8\pi D}\left[1 + \frac{1}{2}\frac{1-v}{1+v} - \frac{a^2}{R^2-a^2}\ln\frac{a}{R}\right] \end{aligned} \tag{A7}$$

Substituting the values of the above constants in Equation A2, the deflection at the radius $r$ can be obtained. The maximum deflection occurs when $r = R$ and is:

$$w = \frac{PR^2}{8\pi D}\left[\left(1 + \frac{1}{2}\frac{1-v}{1+v}\right)\left(\frac{R^2-a^2}{R^2}\right) + \frac{1+v}{1-v}\frac{2a^2}{R^2-a^2}\ln^2\frac{R}{a}\right] \tag{A8}$$

## Appendix B

For the case shown in Fig. 4d, where only the bending moment is distributed along the inner edge,

the shearing force becomes zero, $Q = 0$. That is,

$$\frac{\mathrm{d}}{\mathrm{d}r}\left[\frac{1}{r}\frac{\mathrm{d}}{\mathrm{d}r}\left(r\frac{\mathrm{d}w}{\mathrm{d}r}\right)\right] = 0 \quad \text{(B1)}$$

Integrating Equation B1 twice we obtain:

$$\frac{\mathrm{d}w}{\mathrm{d}r} = \frac{C_1}{2}r + \frac{C_2}{r} \quad \text{(B2)}$$

Integrating again, we obtain the deflection:

$$w = \frac{C_1}{4}r^2 + C_2 \ln\frac{r}{R} + C_3 \quad \text{(B3)}$$

In this case, the boundary conditions become:

$$\begin{aligned} w|_{r=R} &= 0 \\ M_1|_{r=a} &= M \\ M_1|_{r=R} &= 0 \end{aligned} \quad \text{(B4)}$$

Using these equations we find:

$$\begin{aligned} C_1 &= \frac{2Ma^2}{(1+v)D(R^2-a^2)} \\ C_2 &= \frac{MR^2a^2}{(1-v)D(R^2-a^2)} \\ C_3 &= -\frac{MR^2a^2}{2(1+v)D(R^2-a^2)} \end{aligned} \quad \text{(B5)}$$

Putting the values of the above constants in Equation B3 we find:

$$\begin{aligned} w = &-\frac{a^2M(R^2-r^2)}{2(1+v)D(R^2-a^2)} \\ &+\frac{MR^2a^2}{(1-v)D(R^2-a^2)}\ln\frac{r}{R} \end{aligned} \quad \text{(B6)}$$

Superposing case (c) and case (d) in Fig. 4 we can find the deflection under loading as shown in case (b). Using the condition that the slope at $r = a$ is zero, that is, the slope introduced by load $P$ balances that introduced by moment $M$, the moment can be determined using Equation A5 and Equation B2 and the corresponding integration constants. Thus:

$$\begin{aligned} M = &\frac{P}{4\pi[1+v]\dfrac{R^2}{a^2}(1-v)}\left[(1-v)\left(\frac{R^2}{a^2}-1\right)\right. \\ &\left.+2(1+v)\frac{R^2}{a^2}\ln\frac{R}{a}\right] \end{aligned} \quad \text{(B7)}$$

## References


1. R. MCPHERSON, *Surf. Coatings Technol.* **39/40** (1989) 173.
2. R. W. RICE, in "Treatise on Materials Science and Technology", Vol. 11, edited by R. K. MacRone (Academic Press, New York, 1977) pp. 199–381.
3. R. C. ROSSI, *J. Amer. Ceram. Soc.* **51** (1968) 433.
4. N. N. AULT, *ibid.* **40** (1957) 69.
5. M. MOSS, W. L. CYRUS and D. M. SCHUSTER, *Bull. Amer. Ceram. Soc.* **51** (1972) 167.
6. R. C. TUCKER, *J. Vac. Sci. Technol.* **11** (1974) 725.
7. D. FARGEOT, F. PLATON and P. BOCH, *Sci. Ceram.* **9** (1977) 382.
8. P. BOCH, D. FARGEOT, C. GAULT and F. PLATON, *Rev. Int. Hautes Temp. Refract.* **18** (1981) 85.
9. K.-S. SHI, Z.-Y. QIAN and M.-S. ZHUANG, *J. Amer. Ceram. Soc.* **71** (1988) 924.
10. R. MCPHERSON, *Thin Solid Films* **83** (1981) 297.
11. *Idem*, *ibid.* **112** (1984) 89.
12. Y. ARATA, A. OHMORI and C.-J. LI, in Proceedings of the International Symposium on Advanced Thermal Spraying Technology and Allied Coating, Japan High Temperature Society, Osaka, 12–15 May 1988, p. 205.
13. A. OHMORI and C.-J. LI, *Thin Solid Films* **201** (1991) 241.
14. A. OHMORI, C.-J. LI and Y. ARATA, *Trans Jpn. Weld. Res. Inst.* **19** (1990) 99.
15. R. MCPHERSON and P. CHEANG, in "High Performance Ceramic Films and Coatings", edited by P. Vincenzini (Elsevier, Netherlands, 1991) p. 277.
16. P. CHEANG, PhD Thesis, Monash University, (1989).
17. A. M. WAHL and G. LOBO, Jr, *Trans. Amer. Soc. Mech. Eng. Appl. Mech.* **3** (1952) 29.
18. R. MCPHERSON, *J. Mater. Sci.* **15** (1980) 3141.
19. J. F. LYNCH, C. G. RUDERER and W. H. DUCKWORTH, (eds) "Engineering Properties of Selected Ceramic Materials" (American Ceramic Society, Columbus, Ohio, 1966).
20. E. SCHREIBER, *Earth Planetary Sci. Lett.* **7** (1969) 137.



*Received 19 January*
*and accepted 17 September 1996*